Nature Communications

https://doi.org/10.1038/s41467-025-68040-5

Article in Press

Defective cell-autonomous signalling and antigenic polyreactivity of B-cell receptors from chronic lymphocytic leukaemia stereotyped subset 1

Received: 8 October 2024

Accepted: 15 December 2025

Cite this article as: Cocomazzi, P.G., Iatrou, A., Minici, C. *et al.* Defective cell-autonomous signalling and antigenic polyreactivity of B-cell receptors from chronic lymphocytic leukaemia stereotyped subset 1. *Nat Commun* (2025). https://doi.org/10.1038/s41467-025-68040-5

Paolo G. Cocomazzi, Anastasia Iatrou, Claudia Minici, Maria Gounari, Alexandra Theresa Linder, Can Akpınaroğlu, Marco Patrone, Luca Broggini, Michela Frenquelli, Ioannis Sarrigeorgiou, Peggy Lymberi, Georgios Petrakis, Triantafyllia Koletsa, Lydia Scarfò, Andreas Agathangelidis, Hassan Jumaa, Palash C. Maity, Paolo Ghia, Kostas Stamatopoulos & Massimo Degano

Defective cell-autonomous signalling and antigenic polyreactivity of B-cell receptors from chronic lymphocytic leukaemia stereotyped subset 1

Paolo G. Cocomazzi[a,#], Anastasia Iatrou[b,#], Claudia Minici[a,#], Maria Gounari[b], Alexandra Theresa Linder[c], Can Akpınaroğlu[d], Marco Patrone[a], Luca Broggini[e], Michela Frenquelli[f], Ioannis Sarrigeorgiou[g], Peggy Lymberi[g], Georgios Petrakis[h], Triantafyllia Koletsa[h], Lydia Scarfò[f,i], Andreas Agathangelidis[j], Hassan Jumaa[c], Palash C. Maity[d], Paolo Ghia[f,i], Kostas Stamatopoulos[b,*] and Massimo Degano[a,i,*]

[a]Biocrystallography Unit, Department of Immunology, Transplantation and Infectious Diseases, IRCCS Ospedale San Raffaele, 20132 Milano, Italy; [b]Institute of Applied Biosciences, Centre for Research and Technology, 57001 Thessaloniki, Greece; [c]Institute of Immunology, University Hospital of Ulm, 89081 Ulm, Germany; [d]Institute of Experimental Cancer Research, University Hospital of Ulm, 89081 Ulm, Germany; [e]Department of Biosciences, University of Milan, 20133 Milan, Italy; [f]B-cell Neoplasia Unit, Division of Experimental Oncology, IRCCS Ospedale San Raffaele, 20132 Milan, Italy; [g]Immunology Laboratory, Immunology Department, Hellenic Pasteur Institute, Athens, Greece; [h]Pathology Department, School of Medicine, Aristotle University of Thessaloniki, 54124 Thessaloniki, Greece, [i]Faculty of Medicine and Surgery, Università Vita-Salute San Raffaele, 20132 Milano, Italy; [j]Department of Biology, School of Science, National and Kapodistrian University of Athens, 15772 Athens, Greece.

[#] These authors contributed equally

* These authors jointly supervised this work

Corresponding authors: Kostas Stamatopoulos (kostas.stamatopoulos@certh.gr), Massimo Degano (degano.massimo@hsr.it)

Abstract

A shared feature of B-cell receptors (BCRs) expressed on neoplastic B cells from patients with chronic lymphocytic leukaemia (CLL) concerns their continual activation of intracellular signalling without requiring external antigens. This autonomous signalling mechanism has previously been demonstrated to arise from BCR-BCR homotypic interactions in three distinct stereotyped CLL subsets (2, 4 and 169). CLL subset 1 is the second largest stereotyped subset, epitomizing unmutated CLL and known for a particularly aggressive clinical course. Here we show that, despite their significant sequence similarity, BCRs originating from three different subset 1 CLL cases exhibit variations in their combining site structures and associated physicochemical properties. Subset 1 BCRs are characterized by a common reactivity pattern towards various autoantigens, though they maintain distinct receptor-specific characteristics. Analysis of crystal structures of the respective BCR Fab fragments reveals lack of conservation in intermolecular crystal contacts, paralleled by no self-association in solution and incapacity to induce intracellular signalling when expressed in a model B-cell line. These findings suggest that cell-autonomous signalling may not be universally present across all CLL, implying the existence of other mechanisms in sustaining leukemic cell proliferation and CLL progression mediated by BCR signalling.

Introduction

Chronic lymphocytic leukaemia (CLL) is the most common blood cancer and is characterized by the uncontrolled proliferation of $CD5^+$ B cell clones that eventually invade tissues, lymphoid organs and the bone marrow[1,2]. The neoplastic B cells in CLL display an antigen-experienced phenotype, clonally express B-cell receptor (BCR) immunoglobulins (IG) that mostly belong to the IgM class, and a small percentage of cases isotype-switched to IgG or IgA[3]. Disease progression is highly heterogeneous, and, despite advancements in the choice of therapeutic regimens, including combination of fludarabine and alkylating therapy with anti-CD20 monoclonal antibodies or BCL2 antagonists, relapses are frequent[4]. Richter transformation to diffuse large B-cell lymphoma can also occur in 5-10% of CLL cases, with a survival of less than 12 months[5]. B-cell receptor (BCR)-mediated signalling has a crucial role in the natural history of CLL[1,6]. From a clinical perspective, the centrality of the BCR in CLL pathogenesis[7,8] is highlighted by the remarkable efficacy of inhibitors of BCR intracellular signalling such as inhibitors of Bruton's tyrosine kinase (BTK)[9–12] which have revolutionized CLL treatment[7,13]. At the molecular level, the implication of antigen binding to the BCR IG in CLL is underscored by the fact that the impact of somatic hypermutation (SHM) within the IG heavy variable (IGHV) gene sequence dichotomizes CLL in two categories with different biological background and clinical outcome[14]. Compelling evidence for antigen implication also stems from the observation that about 40% of CLL cases, unrelated and from different geographic areas, can be assigned to groups sharing highly homologous, alias stereotyped, BCR IGs[15,16]. Stereotyped BCRs are encoded by heavy and light chain genes that exhibit high levels of sequence identity, and remarkably similar heavy chain

complementarity-determining region 3 (HCDR3), strongly alluding to selection by a restricted set of common antigenic elements[16,17].

The classic notion of self or foreign antigen recognition and binding as a relevant driver in CLL ontogeny has been expanded by the demonstration of cell-autonomous signalling mediated by CLL-derived BCRs[18]. Expression of BCRs from leukaemic cell clones is sufficient to activate a chronic signal that, at least in two stereotyped CLL subsets, is generated through the self-association between BCRs expressed on the same or adjacent leukaemic cells[18,19]. Of note, the affinity and stability of the BCR-BCR homotypic interactions are apparently strongly associated with the clinical outcome of the disease. Indeed, tight interactions were associated with an indolent, slowly progressing disease. Conversely, low-affinity, highly dynamic interactions are characteristic of rapidly proliferating and responsive leukaemic cells. Overall, this notion is exemplified by CLL BCRs belonging to stereotyped subsets 4 and 2, respectively[19]. The structural analysis of BCRs from both indolent (subset 4) and highly aggressive (subset 2) CLL revealed different geometries of BCR-BCR interactions as well as a predominant involvement of either the heavy or light chains in the contacts leading to intracellular signalling[19,20]. These findings highlight the need of extensive studies to understand the plethora of molecular features of the clonotypic BCRs that can underlie the pathogenic antigen-independent signalling and ultimately lead to CLL clonal expansion.

CLL stereotyped subset 1 is the second largest overall, amounting for about 2.5% of all CLL cases and 5% of cases with unmutated IGHV genes (U-CLL)[17]. In CLL subset 1, unmutated IGHV genes of phylogenetic clan I (namely, the homologous IGHV1, IGHV5 and IGHV7 subgroup genes) are exclusively partnered with light chains encoded by the

IGKV1-39/1D-39 gene. CLL subset 1 cells show the highest degree of BCR-dependent proliferation also compared to other U-CLL cases[21], and is clinically aggressive with a short time to first treatment (TTFT) and unfavourable outcome, at least in the era of chemoimmunotherapy[22]. Here, we present the structural, biochemical and cellular analysis of three BCR Fab fragments derived from subset 1 cases utilising different IGHV genes. Despite the high overall homology between the receptors, the limited differences in the amino acid sequences of the respective BCR IG heavy chains are sufficient to modulate differently the shape and properties of the combining site and the reactivity to molecular antigens. Self-association between subset 1 BCR Fabs is not detectable by biophysical methods in solution as well as not apparent from the intermolecular contacts between molecules in the crystals. Most strikingly, this is paralleled by the inability of subset 1 BCRs to mobilize Ca^{2+} ions when expressed in a model B-cell line. Taken together, our study demonstrates that a constitutively active cell-autonomous signalling may not be a unifying feature of all CLL clones, and that at least for a proportion of cases different mechanisms may activate the BCR-mediated signals required for leukaemic cell proliferation and onset of CLL.

Results

Crystal structures of Fab fragments from subset 1 CLL BCRs

We expressed 11 IgM BCR Fab fragments from subset 1 CLL cases in mammalian cells for biochemical and structural studies. The Fabs were purified to near homogeneity using affinity and size exclusion chromatography (SEC), as demonstrated by SDS-PAGE, a single peak eluting from SEC columns (**Supplementary Figure S1**) and the monomodal distribution of the particles in solution in analytical ultracentrifugation (see below). The Fabs derived from three cases using different IGHV chains (P3129: IGHV1-3*01-IGHD6-19*01-IGHJ4*02 heavy chain paired with IGKV1-39*01/1D-39*01-IGKJ2*01 light chain; P10015: IGHV1-2*01-IGHD6-10*01-IGHJ4*02 heavy chain paired with IGKV1-39*01/1D-39*01-IGKJ1*01 light chain; P1173: IGHV5-10-1*03-IGHD6-19*01-IGHJ4*02 heavy chain paired with IGKV1-39*01/1D-39*01-IGKJ2*01 light chain) yielded diffraction-quality crystals that were used to determine the structures using single crystal X-ray diffraction (**Supplementary Table S1**) to gain insights into the landscape of possible combining site structures in subset 1 BCRs.

The three Fabs shared the same overall architecture (**Figure 1A**), with each variable domain folding into the canonical IG fold with a four-stranded (ABDE) juxtaposed to a five-stranded (CC'C''FG) antiparallel β-sheet. The elbow angles of the crystallized Fabs spanned a wide range of values between the independent copies in the asymmetric unit of P3129 (145, 162, 165, and 170°), P10015 (135°) and P1173 (all four, 139°) (**Supplementary Figure S2**), indicating a large degree of flexibility between the variable and constant domains. The portion of the BCR directly involved in binding to antigens, composed of the non-covalently associated heavy and light variable domains (VH and

VL, respectively), were highly similar for all receptors, as judged by the root mean square distances (rmsd) within 0.4 Å (**Supplementary Table S2**). The VH-VL pairing geometry was highly conserved in all the Fab structures here determined, as expected from the strict conservation of the interface residues (**Supplementary Table S3**).

Structural divergence in subset 1 BCR combining sites parallels specific antigenic reactivity

Despite the high sequence similarity between the IGHV1-2, IGHV1-3 and IGHV5-10 genes coupled to the stereotyped HCDR3 sequences (**Figure 1B**) and a common light chain, the combining site of each of the subset 1 BCRs crystallized is characterized by unique structural and biochemical features (**Figure 2A**). Indeed, the HCDR3 loops assume distinct conformations in the three receptors, and this leads to differences in the shape and features of the molecular surface exposed to the solvent and available for antigen recognition. Moreover, despite the conserved canonical structures in the HCDR1 and HCDR2 regions, the differences in amino acid composition further modulate the size, hydrophobicity and charge distribution at the combining sites of the three receptors (**Figure 2B**).

In P3129, the border of the cavity has a positive electrostatic potential, with a major contribution from residue Lys59^{H} from the HCDR2 loop, while the bottom is negatively charged, with the side chain of Glu99^{H} lining the lower portion of the site. Conversely, the combining site of the P10015 receptor lacks the negatively charged patch, and has an overall more neutral character. Indeed, the P10015 combining site is largely lined by neutral, non-polar atoms, due to the absence of both Lys59^{H} and Glu99^{H}, substituted by

Asn and Ala residues, respectively (**Figure 2C**). The binding site in P1173 has an opposite character compared to P3129, with a central region characterized by a strong positive potential. Moreover, the different HCDR3 conformation from that observed in P3129 leads to the protrusion of the shared residue Leu102^{H} inside the binding pocket, allowing its hydrophobic interaction with the side chain phenol ring of Tyr33^{H} to stabilize the loop structure. Consequently, Trp103^{H} also relocates to the outside of the binding site, while Leu104^{H} further strengthens the intermolecular interactions with the LCDR3 loop. In P1173, the side chain of Trp103^{H} stacks with Trp33^{H}, stabilising a yet different conformation of the HCDR3. These findings suggest that BCRs within subset 1 have the potential to interact with shared epitopes, but are also endowed with structural flexibility that can encode specificities directed towards antigens with different chemical properties.

Structural basis for the restricted light chain pairing in subset 1 BCRs

Subset 1 BCRs exclusively express kappa light chains encoded by the IGKV1-39/1D-39 gene. We analysed the VH-VL interface in the P1173 BCR Fab high-resolution structure to clarify the structural basis for this selective association. Formation of the Fab heterodimer is mediated by 14 interchain hydrogen bonds and a total buried surface area of 1,980 Å^2. The VH and VL domains pair through the interaction between 25 heavy chain and 27 light chain residues. The IGHV and HCDR3 regions concur in shaping an interfacing surface characterized by three hydrophobic regions (**Figure 3**). In the central portion of the interface, residues V37^{H}, L45^{H}, F107^{H} and W110^{H} form a hydrophobic pocket that accommodates the side chains of Y36^{L} F99^{L} from the light chain. Residues Y95^{H} and W110^{H} define a pocket optimally complemented by the P44^{L} side chain, also

selecting for a small side chain in the preceding residue. The side chain of $Y87^{L}$ is located between the hydrophobic $L45^{H}$ and $Y95^{H}$ of the heavy chain. Finally, hydrophobic interactions are observed between the side chains of $P62^{H}$ and LCDR3 $P96^{L}$, together with a polar contact between $H97^{L}$ and $E99^{H}$. Besides and beyond the amino acids in the stereotypic HCDR3 sequence that shapes the combining site of the CLL-derived BCRs in subset 1, all the IGHV residues involved in chain pairing are strictly conserved in the other heavy chains found in stereotyped subset 1 CLL BCRs. This finding suggests a preference in subset 1 BCRs for a specific IGKV/IGKJ pairing for stability that is optimally achieved through interactions with the IGKV1-39/1D-39 encoded-light chain. To further corroborate this apparently optimal complementarity suggested by the visual analysis, we evaluated *in silico* the effect of the mutation of IGKV1-39/1D-39-specific amino acids on the stability of the P1173 BCR Fab using the program FoldX [23]. Mutations of residues $Y36^{L}$, $P44^{L}$ (framework), or $Y87^{L}$, $P96^{L}$ and $F99^{L}$ (LCDR3) to alanine to assess the contribution of the side chain-mediated contacts had indeed a destabilizing effect, ranging between 2.34 and 3.71 kcal/mol that is above the standard error for the program (1.0 kcal/mol), thus confirming the complementarity between the heavy and the light chain. Next, we assessed the effect of specific substitutions to amino acids found at the corresponding position in other human IGKV genes and alleles. Mutation of $Y36^{L}$ to phenylalanine, a variation found in alleles of the IGKV1-16, IGKV1D-17, 2-30, IGKV2D-26 and IGKV2D-30 genes, destabilizes the molecule by 1.49 kcal/mol, while its substitution to leucine (found in IGKV2-24) has an even greater variation of 2.24 kcal/mol. Similarly, substitution of $P44^{L}$ with alanine (in IGKV5-2) or serine (IGKV2D-26) decreases the stability by 2.95 or 3.60 kcal/mol, respectively. Thus, the structural analysis of subset

1 BCR Fabs indicates that the heavy and light chains unveiled a finely-tuned complementarity between the heavy and light chains, mediated by residues in heavy and light chain variable domains and both CDR3 regions.

Subset 1 BCRs are polyreactive and display intra-subset diversity

To gain comprehensive insight into the subset 1 BCR reactivity towards potential protein autoantigens, we generated recombinant monoclonal antibodies (rmAbs) from 14 cases (six cases expressing the IGHV1-2, five cases expressing the IGHV1-3 and three cases expressing IGHV5 genes (IGHV5-10-1, n=2; IGHV5-51, n=1); including the three cases for which the Fabs were crystallized) and characterized in-depth their ligand binding profile towards live cells, normal human tissues and various antigenic targets through flow cytometry, ELISA, immunohistochemistry and protein microarrays. All tested subset 1 rmAbs (n=14) bound live HEK293 epithelial cells, albeit with different affinity that indicates intra-subset heterogeneity, with a binding range between 2.6% and 32% as assessed with flow cytometry (**Figure 4A**). Next, we evaluated by ELISA the binding of subset 1 rmAbs, including the three whose Fab structures were determined, to autoantigens that are common targets of autoantibodies as well as CLL-derived BCRs, namely: dsDNA, human skeletal muscle actin, myosin, human thyroglobulin, β-amyloid peptide and the non-self hapten 2,4,6-trinitrophenyl. Again, most of the 14 subset 1 rmAbs tested were reactive towards the autoantigens while showing no binding to the hapten. Distinct behaviours were apparent for different rmAbs (**Figure 4B**), yet no significant differences emerged between groups utilizing the IGHV1-2 vs IGHV1-3 vs IGHV5 genes (**Supplementary Figure S3**). A trend for less pronounced polyreactivity was noted for

subset 1 cases utilizing IGHV5 genes, though not reaching statistical significance. Given that subset 1 BCRs exclusively express heavy chains of the μ isotype, we additionally expressed subset 1 IgM rmAbs and evaluated their reactivity using ELISA assays with the indicated autoantigens and flow cytometry against viable HEK293 epithelial cells. The subset 1 IgM rmAbs exhibited reactivity patterns that were consistent with those observed for the corresponding IgG rmAbs (**Supplementary Figure S4**), confirming their intrinsic autoreactivity irrespective of the heavy chain isotype. This finding supports the view that the structural dissimilarities in the combining sites observed in the crystal structures of the subset 1 BCR Fabs indeed reflect distinct antigenic reactivity. We also investigated the binding profile of the subset 1 rmAbs (n=3, including P1173 crystallized here) through immunohistochemistry in normal tissues, using the CLL rmAbs as primary antibodies (**Figure 4C**). All tested subset 1 rmAbs demonstrated binding to epitopes expressed in several types of lymphocytes in the follicular (mantle and germinal centre) and interfollicular areas, with differences in the intensity of the staining from mild to strong (**Figure 4C**). Moreover, subset 1 rmAbs exhibited positive staining on the squamous cells of the tonsil and the epithelial cells of the appendix (1/3 rmAbs), as well as the tubules or glomeruli of the kidney (2/3 rmAbs), with different levels of immunoreactivity in each tissue. Finally, we evaluated the binding of selected subset 1 rmAbs (n=3) against a variety of autoantigens using a protein microarray chip. Eighteen additional CLL cases belonging to stereotyped subsets 4 (n=3), 111 (n=2), 2/169 (n=4) and 201 (n=6) or non-stereotyped U-CLL (n=2) and M-CLL (n=1) were used for comparisons (**Figure 5**). Protein microarray analysis revealed a reactivity signature of subset 1 rmAbs towards autoantigens that was distinct from that of other CLL stereotyped subsets, giving a weak

positive signal against proteins such as CENP-B, β2-microglobulin (β2m), the nucleosome antigen, Jo-1, PL-7 and fibrinogen IV but with different affinities. Variations in ligand binding affinity were also apparent between the different subset 1 rmAbs tested (Figure 4). We further analysed the reactivity of two subset 1 rmAbs against two antigens showing stronger and weaker binding in the microarrays, fibrinogen IV and β2m (**Figure 5**). Neither antigen showed measurable affinity towards the two rmAbs when using biolayer interferometry or mass photometry. Western blotting analysis, instead, revealed that the subset 1 rmAbs react very weakly with β2m, but strongly with the denatured fibrinogen (**Supplementary Figure S5**), paralleling what observed in the microarray analysis.

Subset 1 CLL BCR Fabs do not form stable homotypic complexes

Patients P3129, P10015 and P1173 experienced progressive CLL with a TTFT of 7.5 months, 5 years and 13 months, respectively. Our previous work showed an apparent association between rapid disease progression and low BCR self-affinity[19], hence we investigated whether the subset 1-derived BCR Fabs also displayed low propensity to dimerization. First, using the software PISA, we analysed the intermolecular Fab-Fab contacts from the three crystal structures to ascertain whether a conserved geometry of homotypic contacts was apparent. The four independent molecules in the P3129 BCR Fab crystals are arranged as dimer of dimers, and each pair of Fabs interacts in a quasi-symmetrical, head-to-head arrangement mediated by the HCDR2 and LCDR1 and LCDR3 regions, burying a total of 415 $Å^2$. In P10015, crystal symmetry leads to a homotrimeric arrangement of molecules mediated by both the light (502 $Å^2$ interface area)

and the heavy chains (250 $Å^2$). The combining site of this receptor is in contact with the Cμ1 domain, specifically the 139-142 loop and the α-helical segment spanning residues 194 to 203, burying a surface of 502 $Å^2$ but forming only one hydrogen bond between the molecules. Finally, none of the intermolecular contacts in the P1173 crystals resembled antibody-antigen interactions, as they did not involve the BCR combining site. Thus, the crystal contacts for both the IGHV1-2, IGHV1-3, and IGHV5-10-1-expressing CLL subset 1 BCR Fabs did not exhibit a conserved modality of self-association between the molecules (**Supplementary Figure S6**). Moreover, the sizes of the protein surfaces buried through the crystal contacts were small and suggestive at best of dynamic, low affinity interactions.

Since the formation of crystals was promoted by organic compounds (polyethylene glycol) or high salt (ammonium sulfate) concentrations that may disrupt weak physiological interactions between the Fab molecules, we further analysed the formation of BCR IG complexes in solution using size-exclusion chromatography (SEC) and analytical ultracentrifugation (AUC). To provide a comprehensive view of the self-association properties of subset 1 BCRs, we performed this analysis in Fabs using the IGHV1-2, IGHV1-3 and IGHV5-10-1 gene products. The recombinant Fabs from 11 distinct subset 1 cases eluted as symmetrical single peaks from SEC columns, indicative of a largely monomeric state when injected at concentrations up to 10 μM (**Supplementary Figure S1**). We further investigated the self-association of BCR-derived Fabs using sedimentation velocity AUC experiments. For all the recombinant BCR Fab fragments, no evidence of dimerization could be obtained with protein concentrations up to 20 μM for any of the recombinant BCR Fab fragments. Indeed, a single, narrow peak at a

sedimentation coefficient of 3.8 S (1 S=10^{-13} s) was observed for all cases in the cumulative *c(s)* deconvolution of the sedimentation curves (**Figure 6**, **Supplementary Figure S7**). For comparison, the subset 4 BCR Fabs that dimerize with a 20 μM K_D showed the concentration-dependent appearance of a second species at 5.0 S in SV-AUC experiments [19]. Thus, the structural and biochemical analysis performed on subset 1 BCR Fabs did not provide any evidence for the formation of stable homotypic complexes in solution.

CLL subset 1 receptors do not activate cell-autonomous signalling

The monomeric state of subset 1 Fabs detected using both SEC and AUC can be consistent with either no homodimerization or the existence of a fast monomer-dimer equilibrium characterized by weak affinity in solution. Nevertheless, the possibility still held that the environment at the cell membrane could strengthen intermolecular interactions and activate BCR intracellular signalling. Indeed, that was the case for the previously studied subset 2 BCRs that showed a weak and dynamic self-association, yet could activate cell-autonomous signalling when expressed in a model B-cell system [19]. Moreover, the interaction surface involved in homotypic contacts may also comprise the heavy chain constant domains that are missing in the Fab portions used in the biochemical and the structural analyses. Thus, to gain further insight into the molecular mechanisms leading to BCR-mediated signals and supporting cell proliferation in subset 1 CLL cases, we examined the cell-autonomous signalling by measuring Ca^{2+} ion cytosolic flux in the pre-B cell line TKO[24]. These cells have a RAG2$^{-/-}$ λ5$^{-/-}$ SLP65$^{-/-}$ genotype, and express a tamoxifen-inducible ER^T-SLP65 chimera. Upon transfection with

the BCR gene rearrangements, the SLP65 protein adaptor function can be induced by addition of 4-hydroxytamoxifen (4-OHT). SLP65 is a central hub of BCR-mediated signal that, among other proteins, activates PLCγ2 to release IP_3 and ultimately allow Ca^{2+} ion flux in the cytosol that can be monitored using cytofluorimetry. TKO cells were transfected with the DNA encoding for the heavy and light chain gene rearrangements of eight different subset 1 receptors expressing the IGHV1-2, IGHV1-3 and IGHV5 genes (**Supplementary Data 1**). No variation in the intracellular Ca^{2+} levels were detectable after SLP65 activation with 4-OHT (**Figure 7**). Instead, BCRs belonging to other stereotyped and non-stereotyped CLL cases induced the characteristic increase in cytosolic ion flux. All subset 1 receptors could signal upon stimulation with an anti-light chain antibody, demonstrating that the BCR IGs were correctly folded and competent for signalling (**Figure 7, Supplementary Figures S8 and S9**). Thus, CLL subset 1 receptors behave differently from the so far characterized CLL-derived BCR IGs, and are unable to initiate antigen-independent cell-autonomous BCR signalling.

A previous study demonstrated that a IGHV1-3$^+$ BCR (UM-CLL4, at the time assigned to subset 1) can signal autonomously without addition of antigen, thus displaying the hallmark autonomous signalling of CLL-associated BCRs[18]. However, the current criteria for subset definition based on HCDR3 identity collocate the UM-CLL4 case in subset 99, which is closely related to subset 1[17]. That said, primary structure alignment highlights that the UM-CLL4 BCR contains one extra amino acid in the HCDR3, preceded by a methionine whose hydrophobic character differs from the hydrophilic asparagine or histidine found at this position in subset 1. Modelling of the UM-CLL4 BCR structure suggests a different arrangement of these amino acids in space (**Supplementary Figure**

S10) that can differentiate the recognition of both intrinsic and external epitopes. Hence, our current findings, showing an inability to activate Ca^{2+} influx in a total of eight subset 1 receptors tested with the TKO cell system, also demonstrate that the higher stringency in subset definition indeed captures molecular diversities that reflect a different BCR-defined reactivity[17].

Discussion

Since its original identification, antigen-independent BCR-mediated cell-autonomous signalling has gained a lot of attention, and has been considered as a CLL hallmark [18,25]. Previous structural studies showed that BCRs from three distinct stereotyped subsets can interact via homotypic BCR-BCR contacts, ultimately initiating intracellular Ca^{2+} ion influx [19,20]. For BCRs derived from subset 2, 4 and 169 cases, cell-autonomous signalling was found to be dependent on BCR-BCR homotypic interactions, involving subset-specific contact residues. These were unveiled by the experimental X-ray structures, since the high concentration of molecules in the crystals for both the strong (for subset 4) and weak (subsets 2 and 169) BCR self-associating cases captured the intermolecular contacts that activate the BCR signalling cascade. The structural analysis of these BCR Fabs highlighted the fact that the contacts between the proteins leading to crystal formation (the so-called crystal contacts, promoted by the crystallization solution) resembled the characteristics of antibody-antigen contacts, and the findings were validated both in solution and in cellular systems.

In the subset 1 BCR Fabs crystals used in the present structural study, the crystal contacts lack the extension and complementarity found in antibody-protein antigen interactions and in the subset 4, 2 and 169 cases, and involve different regions of the proteins in the crystals obtained from three subset 1 cases. Additionally, our analysis in the TKO cells demonstrated that unlike the previously analysed BCRs from other stereotyped or non-stereotyped CLL cases [18], subset 1 BCRs are unable to activate receptor-mediated signals such as the Ca^{2+} ion influx in the absence of additional stimuli. These findings underline the notion that cell-autonomous signalling represents a

mechanism for the BCR-mediated activation in CLL, but should not be assumed for all leukaemic clones. Moreover, although the protein crystal environment can stabilize weak intermolecular interactions, care must be taken in the interpretation and validation of the physiological relevance of the BCR-BCR crystal contacts in the context of cell-autonomous signalling.

Our results show that subset 1 BCR do not establish homotypic contacts capable of triggering intracellular signalling, thus other ligands are likely involved in the activation of the leukaemic clones *in vivo*. Indeed, BCR-mediated signalling is also crucial for the disease progression in subset 1, as demonstrated by the response of patients to the treatment with inhibitors targeting the downstream pathway. While TKO cells offer a standardized system to assess autonomous signaling potential, they lack components of the native B cell microenvironment and may not support engagement by subset 1-specific ligands. Moreover, by analysing the BCR surface expression and intracellular retention, we cannot elucidate the alternate trafficking behaviour of subset 1 BCRs compared to other subsets. Alternative attempts to perform competitive BCR assembly expression in naïve B-cell lines expressing endogenous BCR-positive would be complex due to combinatorial unsuccessful HC-LC pairing that can be distinguished from other means of intracellular retention. Together, these findings warrant further studies aimed at dissecting the mechanistic differences in BCR signaling between self-associating, autonomously active receptors such as those in subset 2, and structurally monomeric but polyreactive receptors exemplified by subset 1.

The classification of stereotyped BCRs in CLL is based on the presence of highly homologous HCDR3 loops, which may be suggestive of a shared exogenous antigen

driving immunoglobulin selection[15,16]. Previous studies aimed at characterizing the subset 1 BCR reactivity using different approaches[26–31], suggesting the nature of several possible ligands. For instance, subset 1 BCRs were shown to react with myosin-exposed apoptotic cells[30], epitopes associated with oxidation[31], histidyl tRNA synthetase[29], and *Streptococcus* and *Enterococcus* strains[28]. The present reactivity studies confirm that subset 1 BCRs can react with diverse macromolecular autoantigens and tissues, and demonstrates specific inter-clonal differences in reactivity patterns. The combining sites of all three subset 1 BCR Fabs here determined contain a cavity bordered by the CDR loops of both the heavy and light chains. The nature of the atoms that line this cavity in each BCR is different due to both the inter-receptor variations in amino acid sequence and the conformation of the HCDR3 loops. The observed differences in the combining site structure and chemical characteristics parallel the differences in autoantigen reactivity, both in specificity and affinity. Nevertheless, the presence of a pocket-like structure in the central region of all combining sites is suggestive of optimal interactions towards a relatively small epitope. Previous studies indicated that CLL subset 1 receptors can bind to oxidized low-density lipoprotein (LDL), specifically with the malondialdehyde (MDA) derivative of LDL [26,27,31]. MDA is a product of lipid peroxidation that is highly reactive and can undergo reactions with several moieties in proteins, including but not limited to lysine residues [32]. Reaction of MDA with collagen and other proteins can yield to several adducts, including 1,3-di(N^{ε}-lysino)-propane. Antibodies able to bind to MDA-modified proteins have been described, and, interestingly, these displayed a high degree of cross-reactivity against diverse MDA-modified polypeptides[33], suggesting that specific recognition of the modified amino acids can be achieved irrespective of the associated

polypeptide. It remains to be experimentally assessed whether subset 1 BCRs can directly be activated through binding to MDA-modified proteins, and further studies will be required to precisely define the molecular determinants that mediate the activation of the subset 1 CLL cells and, ultimately, disease progression.

Within the stereotyped fraction of CLL, subset 1 is typically associated with a short TTFT and poor prognosis[22]. The respective BCRs display a short HCDR3 loop and are invariably composed by one of a few homologous IGHV genes of IGHV clan I coupled to IGKV1-39/1D-39 light chain[16]. The three subset 1 BCR Fab structures here determine the molecular basis for this selective association. First, clan I genes encode for the same amino acids that are crucial for the specific pairing with the subset-restricted IGKV1-39/1D-39 light chain. Second, the amino acid residues from the J gene of each chain perform a dual role in providing a specific chain pairing and shaping of the combining site. Mutation of the contacting amino acids to other residues found in different IG genes resulted in a computed loss of stability. Thus, the combined use of a set of homologous IGHV genes, stereotyped HCDR3, and a specific IGKV/IGKJ gene recombination in CLL subset 1 results in BCRs with shared, specific structural features. Taken together, our analysis provides a structural explanation at the three-dimensional level for the selection of heavy and light chains paired with specific amino acid sequences in both CDR3 regions[34,35]. Another possibility is that a specific antigen-binding architecture is obtained only through this specific gene usage, a hypothesis that could be verified through further experiments upon identification of a tight-binding, specific antigen.

The combining sites of the BCR IGs are shaped by the three-dimensional arrangement of the amino acid residues from the heavy and light chain CDRs. The present structural

analysis shows that these regions in different subset 1 BCR Fabs have specific chemical characteristics due to the differences in the amino acid composition of the HCDR1 and HCDR2 loops and the HCDR3 conformations. While the observed structural differences may be due to the inherent flexibility of the HCDR3 loops in the BCR IG when not bound to an antigen, the variation in amino acid character of the other heavy chain CDR residues also modulates the hydrophobicity and hydrogen bonding possibilities for interaction with ligands. Instead, the light chain conformation is strictly conserved in all three BCR Fabs crystallized, and this may support a central role for the light chain in the natural history of subset 1 clones, either through classic interaction with antigens or with a non-standard superantigenic mechanism.

Notably, the BCRs used in this study showed weak reactivity to the panel of antigens tested compared to other CLL-derived BCRs. Previous studies in animal models showed that the strength of the BCR-antigen interaction modulates the resulting intracellular signal, with strong binding to membrane-bound antigens leading to an anergic B-cell phenotype[36,37]. This finding was also paralleled in the binding affinity and half-life of homotypic complexes between CLL BCRs derived from cells mediating indolent or aggressive disease[19]. It seems thus likely that weak interactions with endogenous antigens may similarly lead to intracellular signals that can promote proliferation.

In conclusion, it is well appreciated that the BCR-mediated signal in CLL cells has a paramount importance in disease progression, and represents a target for therapeutic purposes. The identification of the intrinsic and extrinsic factors leading to its activation has clarified the molecular events involved in the pathology. At the present, the existing data and our present results suggest that BCR activation can take place either through

a) homotypic BCR-BCR interactions, demonstrated in several CLL subsets and non-subsets [18–20], that can range in affinity and stability from low to high; b) strong interactions with very specific antigens, such as BCRs with specificity towards fungi-derived glycans [38] or rheumatoid factors [39,40]; or c) chronic stimulation from the microenvironment, as may be the case for subset 1, subset 111 and other receptors [28,29,31] displaying polyreactivity. Within this framework, the analysis of subset 1 CLL-derived BCRs reinforces the concept that the intracellular signals required for leukaemic cell proliferation may arise not only from the recognition of an internal BCR epitope in a cell-autonomous fashion, but may also derive from the recognition of diverse self-antigen(s). The intra-subset structural differences, paralleled by differences in antigen reactivity, underscore the importance of the integration of three-dimensional analyses with sequence-based CLL BCR stereotypes to assist in patient stratification and clinical management.

Methods

BCR Fab expression and purification

The coding sequences for the IG heavy and light chains of each Fab were cloned into the pcDNA3.1 vector for protein expression in eukaryotic cells. The IG heavy chain was modified to include a tobacco etch virus (TEV) protease recognition sequence followed by a decahistidine peptide at its C-terminus. Expi293F cells were grown in Expi293F expression medium to a final density of $3 \cdot 10^6$ cells/ml, and transfected with the heavy and light chain-encoding plasmids in a 1:2 w/w ratio using PEI MAX 40K. The supernatant was collected after 6 days by centrifugation, filtered through a 0.22 µm filter, loaded on a HisTrap excel 5 mL column attached to an AKTAPure FPLC system (Cytiva) with UV detection (280 nm). The column was washed with 20 column volumes of a buffer composed of 50 mM Tris·HCl pH 7.2 and 1 M NaCl, and eluted with a buffer containing 50 mM Tris·HCl pH 7.2, 0.3 M NaCl, 0.5 M imidazole. The C-terminal affinity peptide was removed by limited proteolysis using recombinant TEV protease, and the Fab was further purified through size exclusion chromatography using a HiLoad 16/600 Superdex 200 prep-grade column and an isocratic elution at 0.5 mL/min. Protein purity was assessed by Coomassie-stained SDS-PAGE, a single peak elution from size-exclusion chromatographic columns and a unimodal distribution of the sedimentation coefficients in analytical ultracentrifugation (Supplementary Figure S4). The concentration of each protein was determined spectrophotometrically using the molar absorption coefficient computed from the amino acid sequence.

Crystal structure determination

Single crystals of the subset 1 Fabs were obtained using the vapour diffusion method, both in batch and sitting drop experiments, mixing equal volumes of the protein and the precipitant solutions. Crystallization and cryoprotection conditions were as follows: P3129 at 10 mg/ml was crystallized from a solution containing 0.1 M sodium potassium tartrate pH 7, 0.1 M magnesium chloride, 20% PEG 3,350, that was supplemented with 15% glycerol for cryoprotection; P10015 at 10 mg/ml was crystallized from a solution containing 0.2 M ammonium succinate pH 7 and 1.5 M ammonium sulfate, and the crystals were transferred to a solution 0.2 M ammonium succinate pH 7, 2 M sodium malonate for cryoprotection; P1173 at 10 mg/ml was crystallized from a solution containing 0.1 M citric acid pH 5 and 20% PEG 6,000, supplemented with 25% glycerol for cryoprotection. Crystals were harvested with nylon loops and transferred rapidly into liquid N_2 where they were kept until data collection.

Monochromatic X-ray diffraction data were measured at the European Synchrotron Radiation Facility beamlines ID30-A1 and ID30B using the oscillation method at 100 K. Data were integrated with AutoProc[41] coupled to XDS[42], scaled and reduced to unique intensities with SCALA[43] and STARANISO[41] using both the spherical and elliptical distribution of the $CC_{1/2}$ to establish the resolution limits for the measured data[44,45]. Initial phases for the P3129 Fab were determined using the molecular replacement technique as implemented in the program Phaser[46], using separately the Fv and Fc fragments from the subset 2 P11475 case BCR Fab (PDB code 5IFH) to locate the four independent Fabs in the asymmetric unit. Non-crystallographic symmetry averaging coupled to phase extension starting from 7.0 Å in DM[47] was employed to remove model bias and produce an electron density map that allowed the rebuilding of the model and the assignment of

the correct amino acid sequence. The model was improved through cycles of manual adjustment into sigma-weighted electron density maps using Coot[48] and automated refinement with a maximum likelihood target as implemented in Phenix[49]. Torsional local NCS restraints were maintained throughout the refinement. Isotropic B factor refinement was coupled to the optimisation of the TLS parameters to model anisotropicity[50]. The paired refinement method was used to assess the maximum resolution of the diffraction data that resulted in the model with the smallest R_{crys}/R_{free} divergence[45]. Stereochemical quality of the model was continuously monitored with Molprobity[51]. The structures of the P10015 and P1173 Fabs were also determined by molecular replacement using the P11475 Fab Fv and Fc domains as search models in Phaser. The refined P3129 structure was used in early stages of refinement of P10015 as a reference model in Phenix to avoid over-refinement. Refinement and model building proceeded as described for the P3129 Fab, and the paired refinement technique was used to judge the resolution limit of the diffraction data to be included. Reflection and coordinates for the three crystal structures have been deposited with the Protein Data Bank with accession codes 9GFG (P3129), 9GFF (P10015) and 9GFH (P1173).

Structural analysis

Structures were visualized with Pymol (http://www.pymol.org). Interaction surfaces between molecules in the crystal including assessment of hydrogen bonds, salt bridges, and measurement of buried surface areas were analysed with PISA[52]. Molecular superpositions and rmsd values were computed with the programs Pymol and LSQKAB[53]. Surface cavities were calculated using CASTp with a 1.4 Å probe radius[54]. Electrostatic

potentials were calculated using PDBQR and APBS[55]. A model of the UM-CLL4 subset 99 BCR was obtained using the ABodyBuilder2 server (https://opig.stats.ox.ac.uk/webapps/sabdab-sabpred/sabpred/abodybuilder2)[56]. The effect of mutations to the VH-VL interface of the P1173 BCR Fab structure was evaluated using the AlaScan and PositionScan modules of the FoldX software[23].

Production of recombinant CLL subset 1 monoclonal antibodies

Total cellular RNA isolated from patient-derived peripheral blood mononuclear cells enriched in the $CD5^{+}CD19^{+}$ CLL population (>85%) was reverse transcribed into complementary DNA. Amplification of IGHV-IGHD-IGHJ and IGK/LV-IGK/LJ BCR gene rearrangements was performed using a mix of leader primers and primers annealing to the constant region. The clonotypic IGHV-IGHD-IGHJ and IGK/LV-IGK/LJ gene rearrangements corresponding to the disease-associated malignant clone were identified by Sanger sequencing, confirming their assignment to stereotyped subset 1 CLL.

Recombinant monoclonal antibodies (rmAbs) were prepared using the pIgγ and pIgκ expression vectors containing the constant regions of the human gamma heavy chain and kappa light chain, respectively, as previously described[57]. For each case, the clonotypic IGHV-IGHD-IGHJ and IGKV-IGKJ gene rearrangements were cloned into the appropriate vector based on the isotype expressed by the respective malignant clone[58]. After the successful construction of the heavy and the light chain plasmids, the identity of the IGHV-IGHD-IGHJ and IGKV-IGKJ gene rearrangements cloned in each plasmid to the corresponding rearrangements expressed by CLL cells was documented by Sanger sequencing prior to the transfection.

For rmAb generation, 10 µg of each vector containing the IG heavy and light chain gene rearrangements were co-transfected into HEK293T cells using linear polyethylenimine (Sigma-Aldrich, USA). Seven days after transfection, the cell culture supernatant was collected and rmAbs were harvested using filter concentrators with a 30 kDa molecular weight cut-off (Merck Millipore, USA). The production of soluble IgG was confirmed by quantitative IgG ELISA (Mabtech Inc., USA) and Western blotting. Recombinant monoclonal antibodies of the IgM isotype used to compare the effect of isotype between IgM and IgG rmAbs, were prepared using the same approach.

IgG1 isotype rmAbs P14197 and P3870 for biochemical studies were individually expressed in Expi293F cell line as described above and elsewhere[59]. Six days after transfection, the clarified cell culture supernatant was loaded onto a 1 mL Protein G pre-packed column (Hitrap MabSelect PrismA, Cytiva #17549852), washed with 20 column volumes of 50 mM Tris pH 8, 150 mM NaCl and the rmAb eluted in 20 mM MES pH 6.6, 3.6 M $MgCl_2$. Positive eluate fractions were pooled and extensively dialyzed against phosphate buffer saline (PBS) to remove excess $MgCl_2$. The rmAbs were further purified by size exclusion chromatography as above in the PBS running buffer.

Antigen reactivity

Polystyrene microtiter plates were coated for 1 hour at 37°C followed by overnight incubation at 4˚C with G-actin (10 µg/ml), myosin (10 µg/ml), TNP–BSA (10 µg/ml), thyroglobulin (10 µg/ml), β-amyloid peptide (2 µg/ml), trinitrophenyl (TMP)-BSA (10 µg/ml) in 0.1 M carbonate/bicarbonate buffer at pH 9.6, or native DNA (10 µg/ml) in PBS pH 6.85. Next, plates were washed thoroughly with PBS and then saturated for 1 hour at

37°C with PBS containing 1% BSA (Sigma-Aldrich, USA). CLL rmAbs were used as primary antibodies in duplicates diluted in PBS containing 0.1% Tween and 1% BSA (PBS-T-BSA) at a concentration of 15 µg/ml (for both IgG and IgM rmAbs) and were incubated with each immobilized antigen of the panel for 2 hours at 37°C. Next, alkaline phosphatase-conjugated anti-human IgG (Sigma-Aldrich, USA) was used as secondary antibody at a concentration of 600 ng/ml in PBS-T-BSA for 2 hours at 37°C, followed by washes with PBS containing 0,1% Tween (PBS-T) and PBS alone. The enzyme's soluble chromogenic substrate p-nitrophenyl phosphate disodium hexahydrate (pNPP) (Sigma-Aldrich, USA) was then added, and optical density (OD) was measured at 405 nm on a TECAN-Spark multimode microplate reader (Tecan, Switzerland).

Flow cytometry

$50x10^4$ cells were resuspended in 100 µl PBS-FBS 1% and incubated with CLL rmAbs (25 µg/ml) for 1 hour at room temperature. PE Mouse Anti-Human Igκ Light Chain (BD Biosciences, USA) was used as a secondary antibody. Before data acquisition, cells were exposed to the 7-AAD viability dye. Data were collected using an Attune NxT Flow Cytometer (ThermoFischer Scientific, USA) and analysed with the FlowJo software (Flowjo, LLC, USA). The mean binding of each rmAb was calculated after 2-3 independent experiments.

Immunohistochemical studies

All immunohistochemical stains were performed on 4 µm whole tissue sections mounted on Superfrost slides. The sections were dried at 60ºC for 12 hours, followed by rinsing in

xylene for 10 minutes and alcohol solutions (100%, 96% and 70%), each for 5 minutes. Then, they were covered with TBS buffer for 5 minutes. Antigen heating retrieval with citrate buffer solution at pH 9 was performed for 10 minutes. Then, the blocking agent IgG Fab fragment (Jackson ImmunoResearch, USA) (100 μg/ml) was used for 1 hour in order to block any endogenous IgG. Primary CLL rmAbs (20 μg/ml) were introduced for 1 hour followed by incubation with the secondary IgG antibody at room temperature. Then, the peroxidase-labeled EnVision system protocol was performed according to the manufacturer's instructions (Dako Envision Flex System) with 3,3'-diaminobenzidine (DAB) used as the chromogen and hematoxylin as counterstain. Known positive control sections were used, as well as negative controls omitting the primary antibody. Staining for each slide was evaluated by experienced pathologists, not informed about the molecular and clinical data. The pattern of staining, the different types of cells stained and the level of staining intensity were evaluated and graded. The evaluation was performed with a Nikon Eclipse E600 microscope and microphotographs were captured with a Nikon DS-Fi1-mounted to microscope camera.

Protein microarrays

The autoantigen array bearing the testing autoantigens and 4 control proteins were printed in duplicates onto nitrocellulose film slides. The primary antibodies (CLL rmAbs) were incubated with the autoantigen arrays. Stringent washing conditions were used to ensure optimum binding specificity. Bound autoantibodies were measured with Cy3-conjugated anti-human IgG (1:2000, Jackson ImmunoResearch Laboratories, USA),

using a GenePix Microarray 4000B scanner. The GenePix Pro Microarray Image Analysis v7.0 software was used to obtain raw data.

Unsupervised analysis was performed to investigate clusters formed between samples and identify antigens with significant differences amongst the sample metadata. The input of the analysis is a matrix containing antigen reactivity with each row of the matrix corresponding to a different antigen and each column representing a sample. To avoid any biases that could arise from variation in the technology, the input table was normalized based on the CPM (counts per million) methodology. After normalization, hierarchical clustering was applied both on the samples of the same patient (columns of the table) and the antigens (rows of the table). For this process, the Euclidean distance was used to create the distance matrices, and the Ward D2 method[60] for the clustering of the related observations (samples and antigens).

Mass photometry

Mass photometry experiments were done using a Refeyn OneMP instrument (Oxford, UK). The experiments were performed using microscope coverslips, which were assembled into the flow chamber, and silicone gaskets were positioned on the glass surface for sample loading to hold the sample drops with 4 × 4 wells prior to measurements. Contrast-to-mass calibration was achieved by measuring the contrast of tyroglobuline (660 kDa), beta-amylase (224 kDa, 112 kDa, 56 kDa), and bovine serum albumin (66.5 kDa). Calibration was applied to each sample measurement to calculate the molecular mass of each histogram distribution during analysis. For the experiment, P14197, P3870, and fibrinogen were diluted to a final concentration of 10 nM in PBS pH

7.4. For complexes, P14197 was incubated with fibrinogen at a 3:1 molar ratio for 30 min at 26°C. Similarly, P3870 and fibrinogen were incubated at a 1:3 molar ratio for 30 min at 26°C. The mixtures were then diluted to 10 nM and analysed. For data acquisition, movies of 60 s duration with 2800 frames were recorded using Refeyn AcquireMP 2023 R1 software in normal measurement mode with regular image acquisition settings. All mass photometry movies of each measurement were processed and analysed by Refeyn DiscoverMP v2023 R2 software, and Gaussian curves were fit to each histogram distribution, and the mass (kDa), sigma (kDa) and counts were determined.

Bio-layer interferometry

BLI was performed using single-use Protein A sensors on an eight-channel Octet RED 96e instrument according to manufacturer's protocols (Fortebio). Assays were performed in PBS pH 7.4, supplemented with 0.05% Tween-20 to reduce non-specific binding. The sensors were divided into two sets, sample and reference sensors. The sample sensors were loaded with either antibody P14197 or P3870 (immobilization level of 1 nm) while reference sensors were not. All sensors were dipped into β2m at a concentration of 10 µM. For kinetics experiments, P14197 was immobilized on Protein A sensors at immobilization level of 1 nm and then dipped into β2m solutions. β2m was prepared at serial dilutions from 5 µM to 0.15 µM. Final presented curves were reference-subtracted Savitzky-Golay filtered, as implemented in the Octet® Analysis Studio Software (Sartorius). GraphPad Prism 9.0 software (CA, USA) was used for visualization and graph generation.

Immunoblotting

Human Fibrinogen (Merck #F3879) or purified β2-microglobulin at 200 and 50 ng/lane, respectively, were assayed by immunoblot along with 20 µg total protein crude HeLa cell lysate. Mouse MAb anti-Fibrinogen clone C-20 (Santa Cruz Biotechnology #sc-18029, 1:1000 dilution), rabbit MAb anti-CD247 clone E1L3N (Cell Signaling Technology #13684, 1:1000 dilution) and rabbit MAb anti-β2-microglobulin clone D8P1H (Cell Signaling Technology #12851, 1:1000 dilution) were used as controls. Both P14197 and P3870 were assayed at 5 µg/mL as primary antibodies and revealed with a goat anti-Human Kappa-HRP conjugate (SouthernBiotech #2060-05, 1:5000 dilution). Chemiluminescence (SuperSignal West Dura, Thermo Fisher Scientific #34076) was acquired at a Chemidoc Touch (BioRad).

Analytical ultracentrifugation

Sedimentation velocity (SV) experiments were performed using a Beckman/Coulter XL-I analytical ultracentrifuge equipped with a double centrepiece and sapphire windows. Protein concentrations were adjusted to 0.1, 0.2, 0.4, 0.7 and 1.0 mg/mL in a buffer composed of 20 mM Tris (pH 7.4) and 150 mM NaCl. Samples were centrifuged at 72,756 x g at a temperature of 20 °C for 16 hours, and radial absorbance plots were recorded every 4 minutes. The experimental curves were deconvoluted to *c(s)* histograms to determine the distribution of molecular species in solution using the program SEDFIT[61].

Design and expression of BCR for Ca^{2+} influx measurements

Immunoglobulin heavy chain (HC) and light chain (LC) sequences obtained from 8 CLL subset 1 cases were cloned into pMIGw retroviral vector for the expression of human IgM BCR followed by an internal ribosomal entry sequence (IRES) coupled green fluorescent protein (GFP) reporter as previously described[25,62]. Unlike previous split GFP-based dual vector systems, a single p2A-based self-cleavable bi-cistronic plasmid was used for the stoichiometric expression of either the κ or λ-LC along with the μHC. To ensure normal BCR expression and membrane localization, the respective endogenous IGHV and IGK/LV germline 5' leader sequences (retrieved from the NCBI Gene databases) were cloned upstream the mature polypeptide-coding sequences. Among the eight receptors, representing three classes of clan I IGHV gene segments associated to subset #1, namely IGHV1-2 (three cases), IGHV1-3 (three cases), and IGHV5 (IGHV5-10-1 and IGHV5-51), two receptors namely P3129 (IGHV1-3*01) and P10015 (IGHV1-2*02) were crystallized. The sample P1173 (IGHV5-10-1*03), despite being crystallized, was not tested in the TKO system. Instead, we analysed the identically VDJ rearranged sample P5029 (IGHV5-10-1*03). Furthermore, P14197 (IGHV1-2*02), although identified as one of the most polyreactive subset 1 antibodies, was not tested in TKO cells, instead we analysed the two other strongly autoreactive similar VDJ rearranged receptors P10015 and P3870. Retroviral transduction was performed as previously described[63,64]. In brief, HEK293T or Phoenix-Eco cells were transfected with BCR encoding retroviral plasmids together with ecotropic packaging helper plasmid using the GeneJuice Transfection Reagent (Millipore) as recommended by the manufacturer's protocol. Culture supernatants containing the matured retroviral particles were collected 72 hours after transfection and used for the subsequent transduction of ERT2-SLP65-expressing TKO

cells by the spin-infection method in presence of 5 µg/ml polybrene (Millipore). BCR expression was evaluated four to five days after viral transduction by measuring the percentage of the GFP-positive cells and surface FACS staining of the membrane-bound IgM molecule with biotinylated anti-λ or -κ LC antibodies (Southern Biotech) followed by Streptavidin PE-Cy7, and PerCP-Cy5.5 anti-µ HC antibody (BioLegend).

Intracellular Ca^{2+} influx measurements.

Ca^{2+} mobilization analyses were performed as described[62]. In brief, $1x10^6$ transduced TKO cells expressing ERT2-SLP65 were loaded with 5 µg/ml Indo-1, AM (Invitrogen), a high affinity, intracellular Ca^{2+} indicator, with 0.05% Pluronic™ F-127 (Invitrogen). Induction of ERT2-SLP65 function was performed by the addition of 4µM 4-Hydroxytamoxifen (4-OHT) (Sigma-Aldrich). To confirm BcR signaling competence, cells were treated with 4-OHT and 5 µg/mL of goat anti-human IgM or anti-human κ/λ antibodies (Southern Biotech) resulting in BCR cross-linking. All FACS measurements were performed on the BD LSRFortessa™ Cell Analyzer (BD Biosciences) equipped with a UV laser and temperature-controlled tube holder for live cell-based assays.

Statistical analysis

FACS data were analysed with FlowLogic (version 8.4). Area under the curve (AUC) and kinetics were calculated by the software. Statistical analysis was performed using the GraphPad Prism software (version 10.2.3). One-Way ANOVA was performed with Welch's approximation followed by Dunnett's T3 multiple comparison post-test.

Significance of mean to mean are shown as (ns; *p<0.05; **p<0.01; ***p<0.001; ****p<0.0001).

Patient data

The subset 1 CLL patients' clinical data, together with the molecular characteristics of the B cells whose BCRs were analysed in the present study, are reported in the Supplementary Table S4.

Data availability.

The crystallographic data and refined structured have been deposited with the Protein Data Bank (PDB codes 9GFF (P10015), 9GFG (P3129), 9GFH (P1173). The protein microarray data have been deposited in Science Data Bank under the accession codes CSTR: 31253.11.sciencedb.30441 (https://cstr.cn/31253.11.sciencedb.30441) and DOI: 10.57760/sciencedb.30441 (https://doi.org/10.57760/sciencedb.30441). Patient data and BCR sequences are available as supplementary information. All other data is available from the authors upon reasonable request.

References

1. Scarfò, L., Ferreri, A. J. M. & Ghia, P. Chronic lymphocytic leukaemia. *Crit. Rev. Oncol. Hematol.* **104**, 169–182 (2016).
2. Ghia, P., Ferreri, A. M. & Caligaris-Cappio, F. Chronic lymphocytic leukemia. *Crit. Rev. Oncol. Hematol.* **64**, 234–246 (2007).

3. Efremov, D. G., Ivanovski, M., Batista, F. D., Pozzato, G. & Burrone, O. R. IgM-producing chronic lymphocytic leukemia cells undergo immunoglobulin isotype-switching without acquiring somatic mutations. *J Clin Invest* **98**, 290–298 (1996).
4. Jain, N., Wierda, W. G. & O'Brien, S. Chronic lymphocytic leukaemia. *Lancet* S0140-6736(24)00595–6 (2024) doi:10.1016/S0140-6736(24)00595-6.
5. Jain, N. & Keating, M. J. Richter transformation of CLL. *Expert Rev Hematol* **9**, 793–801 (2016).
6. Burger, J. A. & Chiorazzi, N. B cell receptor signaling in chronic lymphocytic leukemia. *Trends Immunol* **34**, 592–601 (2013).
7. Burger, J. A. & Wiestner, A. Targeting B cell receptor signalling in cancer: preclinical and clinical advances. *Nat Rev Cancer* **18**, 148–167 (2018).
8. Ten Hacken, E., Gounari, M., Ghia, P. & Burger, J. A. The importance of B cell receptor isotypes and stereotypes in chronic lymphocytic leukemia. *Leukemia* **33**, 287–298 (2019).
9. Byrd, J. C. *et al.* Ibrutinib versus ofatumumab in previously treated chronic lymphoid leukemia. *N. Engl. J. Med.* **371**, 213–223 (2014).
10. Burger, J. A. *et al.* Safety and activity of ibrutinib plus rituximab for patients with high-risk chronic lymphocytic leukaemia: a single-arm, phase 2 study. *Lancet Oncol.* **15**, 1090–1099 (2014).
11. de Claro, R. A. *et al.* FDA Approval: Ibrutinib for Patients with Previously Treated Mantle Cell Lymphoma and Previously Treated Chronic Lymphocytic Leukemia. *Clin. Cancer Res.* **21**, 3586–3590 (2015).

12. Byrd, J. C. *et al.* Targeting BTK with ibrutinib in relapsed chronic lymphocytic leukemia. *N Engl J Med* **369**, 32–42 (2013).
13. Barr, P. M. *et al.* Up to 8-year follow-up from RESONATE-2: first-line ibrutinib treatment for patients with chronic lymphocytic leukemia. *Blood Adv* **6**, 3440–3450 (2022).
14. Hamblin, T. J., Davis, Z., Gardiner, A., Oscier, D. G. & Stevenson, F. K. Unmutated Ig V(H) genes are associated with a more aggressive form of chronic lymphocytic leukemia. *Blood* **94**, 1848–1854 (1999).
15. Agathangelidis, A. *et al.* Stereotyped B-cell receptors in one-third of chronic lymphocytic leukemia: a molecular classification with implications for targeted therapies. *Blood* **119**, 4467–4475 (2012).
16. Stamatopoulos, K. *et al.* Over 20% of patients with chronic lymphocytic leukemia carry stereotyped receptors: Pathogenetic implications and clinical correlations. *Blood* **109**, 259–270 (2007).
17. Agathangelidis, A. *et al.* Higher-order connections between stereotyped subsets: implications for improved patient classification in CLL. *Blood* **137**, 1365–1376 (2021).
18. Dühren-von Minden, M. *et al.* Chronic lymphocytic leukaemia is driven by antigen-independent cell-autonomous signalling. *Nature* **489**, 309–312 (2012).
19. Minici, C. *et al.* Distinct homotypic B-cell receptor interactions shape the outcome of chronic lymphocytic leukaemia. *Nat Commun* **8**, 15746 (2017).

20. Gemenetzi, K. *et al.* HIGHER ORDER IMMUNOGLOBULIN REPERTOIRE RESTRICTIONS IN CLL: THE ILLUSTRATIVE CASE OF STEREOTYPED SUBSETS #2 AND #169. *Blood* (2020) doi:10.1182/blood.2020005216.
21. Del Giudice, I. *et al.* Stereotyped subset #1 chronic lymphocytic leukemia: a direct link between B-cell receptor structure, function, and patients' prognosis. *Am J Hematol* **89**, 74–82 (2014).
22. Baliakas, P. *et al.* No improvement in long-term survival over time for chronic lymphocytic leukemia patients in stereotyped subsets #1 and #2 treated with chemo(immuno)therapy. *Haematologica* **103**, e158–e161 (2018).
23. Schymkowitz, J. *et al.* The FoldX web server: an online force field. *Nucleic Acids Res* **33**, W382-388 (2005).
24. Meixlsperger, S. *et al.* Conventional light chains inhibit the autonomous signaling capacity of the B cell receptor. *Immunity* **26**, 323–333 (2007).
25. Maity, P. C. *et al.* IGLV3-21*01 is an inherited risk factor for CLL through the acquisition of a single-point mutation enabling autonomous BCR signaling. *Proc Natl Acad Sci U S A* **117**, 4320–4327 (2020).
26. Lanemo Myhrinder, A. *et al.* A new perspective: molecular motifs on oxidized LDL, apoptotic cells, and bacteria are targets for chronic lymphocytic leukemia antibodies. *Blood* **111**, 3838–3848 (2008).
27. Bergh, A.-C. *et al.* Silenced B-cell receptor response to autoantigen in a poor-prognostic subset of chronic lymphocytic leukemia. *Haematologica* **99**, 1722–1730 (2014).

28. Hatzi, K. *et al.* Chronic lymphocytic leukemia immunoglobulins display bacterial reactivity that converges and diverges from auto-/poly-reactivity and IGHV mutation status. *Clin Immunol* **172**, 44–51 (2016).
29. Gounari, M. *et al.* Excessive antigen reactivity may underlie the clinical aggressiveness of chronic lymphocytic leukemia stereotyped subset #8. *Blood* **125**, 3580–3587 (2015).
30. Chu, C. C. *et al.* Chronic lymphocytic leukemia antibodies with a common stereotypic rearrangement recognize nonmuscle myosin heavy chain IIA. *Blood* **112**, 5122–5129 (2008).
31. Catera, R. *et al.* Chronic lymphocytic leukemia cells recognize conserved epitopes associated with apoptosis and oxidation. *Mol Med* **14**, 665–674 (2008).
32. Ferreira, H. B. & Domingues, M. R. Oxidized phospholipid-protein adducts: The future targets of interest. *Arch Biochem Biophys* **754**, 109956 (2024).
33. Grönwall, C. *et al.* Autoreactivity to malondialdehyde-modifications in rheumatoid arthritis is linked to disease activity and synovial pathogenesis. *J Autoimmun* **84**, 29–45 (2017).
34. Widhopf, G. F., II *et al.* Nonstochastic pairing of immunoglobulin heavy and light chains expressed by chronic lymphocytic leukemia B cells is predicated on the heavy chain CDR3. *Blood* **111**, 3137–3144 (2008).
35. Stamatopoulos, K. *et al.* Immunoglobulin light chain repertoire in chronic lymphocytic leukemia. *Blood* **106**, 3575–3583 (2005).
36. Taylor, J. J. *et al.* Deletion and anergy of polyclonal B cells specific for ubiquitous membrane-bound self-antigen. *J Exp Med* **209**, 2065–2077 (2012).

37. Hippen, K. L. *et al.* In vivo assessment of the relative contributions of deletion, anergy, and editing to B cell self-tolerance. *J Immunol* **175**, 909–916 (2005).
38. Hoogeboom, R. *et al.* A mutated B cell chronic lymphocytic leukemia subset that recognizes and responds to fungi. *J Exp Med* **210**, 59–70 (2013).
39. Hoogeboom, R. *et al.* A novel chronic lymphocytic leukemia subset expressing mutated IGHV3-7-encoded rheumatoid factor B-cell receptors that are functionally proficient. *Leukemia* **27**, 738–740 (2013).
40. Kostareli, E. *et al.* Antigen receptor stereotypy across B-cell lymphoproliferations: the case of IGHV4-59/IGKV3-20 receptors with rheumatoid factor activity. *Leukemia* **26**, 1127–1131 (2012).
41. Vonrhein, C. *et al.* Data processing and analysis with the autoPROC toolbox. *Acta Crystallogr. D Biol. Crystallogr.* **67**, 293–302 (2011).
42. Kabsch, W. XDS. *Acta Crystallogr. D Biol. Crystallogr.* **66**, 125–132 (2010).
43. Evans, P. Scaling and assessment of data quality. *Acta Crystallogr D Biol Crystallogr* **62**, 72–82 (2006).
44. Evans, P. R. & Murshudov, G. N. How good are my data and what is the resolution? *Acta Crystallogr. D Biol. Crystallogr.* **69**, 1204–1214 (2013).
45. Karplus, P. A. & Diederichs, K. Linking crystallographic model and data quality. *Science* **336**, 1030–1033 (2012).
46. McCoy, A. J. *et al.* Phaser crystallographic software. *J Appl Crystallogr* **40**, 658–674 (2007).
47. Cowtan, K. & Main, P. Miscellaneous algorithms for density modification. *Acta Crystallogr. D Biol. Crystallogr.* **54**, 487–493 (1998).

48. Emsley, P., Lohkamp, B., Scott, W. G. & Cowtan, K. Features and development of Coot. *Acta Crystallogr D Biol Crystallogr* **66**, 486–501 (2010).
49. Adams, P. D. *et al.* The Phenix software for automated determination of macromolecular structures. *Methods* **55**, 94–106 (2011).
50. Winn, M. D., Isupov, M. N. & Murshudov, G. N. Use of TLS parameters to model anisotropic displacements in macromolecular refinement. *Acta Crystallogr. D Biol. Crystallogr.* **57**, 122–133 (2001).
51. Chen, V. B. *et al.* MolProbity: all-atom structure validation for macromolecular crystallography. *Acta Crystallogr. D Biol. Crystallogr.* **66**, 12–21 (2010).
52. Krissinel, E. Stock-based detection of protein oligomeric states in jsPISA. *Nucleic Acids Res.* **43**, W314-319 (2015).
53. Kabsch, W. A solution for the best rotation to relate two sets of vectors. *Acta Cryst A* **32**, 922–923 (1976).
54. Tian, W., Chen, C., Lei, X., Zhao, J. & Liang, J. CASTp 3.0: computed atlas of surface topography of proteins. *Nucleic Acids Res* **46**, W363–W367 (2018).
55. Jurrus, E. *et al.* Improvements to the APBS biomolecular solvation software suite. *Protein Sci* **27**, 112–128 (2018).
56. Abanades, B. *et al.* ImmuneBuilder: Deep-Learning models for predicting the structures of immune proteins. *Commun Biol* **6**, 1–8 (2023).
57. Wardemann, H. *et al.* Predominant autoantibody production by early human B cell precursors. *Science* **301**, 1374–1377 (2003).

58. Hervé, M. *et al.* Unmutated and mutated chronic lymphocytic leukemias derive from self-reactive B cell precursors despite expressing different antibody reactivity. *J Clin Invest* **115**, 1636–1643 (2005).
59. Patrone, M. & Degano, M. Recombinant Production of B-Cell Receptor Fab Fragments from Chronic Lymphocytic Leukemia in Mammalian Cells for Structural and Biochemical Studies. *Methods Mol Biol* **2909**, 103–118 (2025).
60. Maza, E., Frasse, P., Senin, P., Bouzayen, M. & Zouine, M. Comparison of normalization methods for differential gene expression analysis in RNA-Seq experiments: A matter of relative size of studied transcriptomes. *Commun Integr Biol* **6**, e25849 (2013).
61. Schuck, P. Size-distribution analysis of macromolecules by sedimentation velocity ultracentrifugation and Lamm equation modeling. *Biophys J* **78**, 1606–1619 (2000).
62. Nicolò, A., Linder, A. T., Jumaa, H. & Maity, P. C. The Determinants of B Cell Receptor Signaling as Prototype Molecular Biomarkers of Leukemia. *Front Oncol* **11**, 771669 (2021).
63. Iype, J. *et al.* Differences in Self-Recognition between Secreted Antibody and Membrane-Bound B Cell Antigen Receptor. *J Immunol* **202**, 1417–1427 (2019).
64. Mazzarello, A. N. *et al.* B cell receptor isotypes differentially associate with cell signaling, kinetics, and outcome in chronic lymphocytic leukemia. *J Clin Invest* **132**, e149308 (2022).

Acknowledgments. Supported by research grants from Italian Association for Cancer Research AIRC IG17032 and IG25764 (M.D.), WWCR 19-0096 (M.D.), Italian Ministry of Health Ricerca Finalizzata bando 2018 RF-2018-12368231 (P.G. and M.D.). P.C.M. is supported by the Fritz Thyssen Foundation Grant 10.23.1.012MN and his position is supported by DFG CRC1279 (project B01 to C. Buske). A.I. is a recipient of a PhD Fellowship by the Hellenic Foundation for Research and Innovation (Grant No #10737). The authors thank drs. Massimo Alessio and Monica Casucci for the generous gift of the anti-fibrinogen and anti-CD274 antibodies, and lab members for discussions. We acknowledge the European Synchrotron Radiation Facility (ESRF) for provision of synchrotron radiation and would like to thank David Flot for assistance and support in using beamlines ID30-A1 and ID23-1.

Author contributions. The study was conceived by PG, KS and MD; PGC, CM and MD determined the crystal structures; PGC, MP, LB and CM performed the biochemical analysis; AI, MG, AA and KS performed immunogenetic analyses; PL, IS, AI and KS performed the antigen reactivity experiments; GP and TK performed the immunohistochemical analysis; CA, AL, HJ and PCM performed the experiments and analysed the BCR signalling data; MF, LS and KS provided patient data; PG and MD were responsible for funding acquisition; PG, KS and MD supervised the research. MD drafted the manuscript with contribution from all authors.

Competing interest statement. The authors declare no competing interest.

Figure Legends

Figure 1. Structure of Fabs derived from subset 1 CLL BCRs. **A**, Overview of the subset 1 Fab structure, with the IGKV1-39/1D-39 light chain coloured pink and the heavy chain coloured light blue. The secondary structure elements are shown as arrows (β-strands) and ribbons (α-helices). The complementarity-determining regions of the heavy chain are coloured limon (HCDR1), lime (HCDR2) and green (HCDR3), and orange (LCDR1), magenta (LCDR2) and red (LCDR3). **B**, Alignment of the heavy chains of the P3129, P10015 and P1173 BCR Fabs, and the IGHV1-39/1D-39 amino acid sequences of the BCRs are shown in one-letter code. CDR regions are boxed following the same colour pattern as in panel A, as indicated. Residues in P10015 differing from P3129 are shown in bold, the ones in P1173 in blue.

Figure 2. Structural divergence in subset 1 BCR Fabs. **A**, Superposition of the variable domains from the P3129, P10015 and P1173 receptors. The light chains are coloured pink and the heavy chains sky blue, with the HCDR3s in light blue (P3129), marine (P10015) and cyan (P1173), respectively. The view, representing the point of view of a viewer looking towards the BCR binding site, is maintained in all panels of the figure. **B**, molecular (solvent-excluded) surfaces of the three subset 1 Fabs coloured in a blue-white-red scale according to electrostatic potential. Blue represents positive (5 kT), red negative (-5kT) and white neutral electrostatic potential. Differences in shape and charge are apparent in the three receptors. **C**, semitransparent molecular surfaces of the three BCRs with the side chains of the residues contributing to the combining site of each receptor shown as sticks.

Figure 3. Complementarity between the subset 1 heavy chains and the IGKV1-39/1D-39 light chain. The molecular surfaces of the VH domain of the P1173 BCR Fab (light blue), with the side chains of the residues involved in intermolecular contacts shown as sticks, evidences the presence of distinct pockets. These pockets are lined by residues specifically encoded by the IGHV1, IGHV5, and IGHV7 genes (shown as red sticks) and by the stereotyped HCDR3 (dark green), and are optimally complemented in size and character by amino acid residues of the IGKV1-39/1D-39 light chain. The light chain is shown as a thin ribbon, and parts of the structure have been omitted for clarity. The molecule is oriented with the combining site of the BCR is on the top part of the figure.

Figure 4. Antigen reactivity of stereotyped subset 1 rmAbs. A, Violin + box plots with overlaid individual data points (dots) showing binding of subset 1 rmAbs to HEK293 cells detected with PE anti-human kappa light chain. Center line: median; box: Q1-Q3; whiskers: min-max within 1.5×IQR; threshold: dashed line at 2.5. Sample sizes (n): RS038 n=3; GM056 n=2; P5092 n=2; P3073 n=3; P3870 n=3; P14197 n=3; P23728 n=3; P3560 n=2; P5220 n=3; P10015 n=3; P3129 n=3; P10029 n=3; P8377 n=2; P1173 n=3. B-C, Representative polyreactivity ELISA tests of subset 1 rmAbs. Reactivity against (B) dsDNA and (C) actin was tested. In all ELISAs CLL rmAbs were used, in duplicates, as primary antibodies. Each bar corresponds to the mean OD value. The cut-off value of the weak positivity is indicated by dotted horizontal lines. D, Reactivity of a representative CLL subset 1 rmAb (GM056) in the kidney and the lymph node. In the renal biopsy (original magnification x200), the rmAb showed very positive staining in glomeruli and

tubules. In the lymph node (original magnification x100), the rmAb recognized some lymphocytes in follicular and interfollicular areas. Representative images from 2 independent IHC experiments performed on 2 independent tissue specimens on different days, with similar results. In all panels the negative control of the staining used for comparisons is included in the black-boxed inset.

Figure 5. Reactivity against various autoantigens was tested using a protein microarray chip. Each row of the heat map corresponds to a different antigen while every column represents a sample. Heat maps are depicted with dark red representing the highest relative reactivity level, and white the absence of relative antibody activity level, as indicated in the inset.

Figure 6. Undetectable self-association of subset 1 CLL BCR Fabs in solution. SV-AUC analysis of the P3129, P10015 and P1173 BCR Fabs using protein concentrations up 20 μM (~ 1.0 mg/mL) demonstrate the presence of a single, monomeric Fab species in solution (one representative experiment shown for each Fab, n=3). The analysis of seven other subset 1 and one subset 4 BCR Fabs are reported in Supplementary Figure S7.

Figure 7. Defective cell-autonomous signalling mediated by subset 1 BCRs. **A**, Ca^{2+} release kinetics of P3129, P5092 and P10015 (left panels) compared to controls derived from CLL#2, healthy donor (HD) and no BCR (right panels) upon addition of 4-OHT ± anti-Igκ/λ antibody, revealing autonomous BCR signaling and BCR signaling capacity, respectively. BCR isotypes, associated light chain and VDJ annotations are depicted for

each sample. Addition of 4-OHT ± anti-Igκ/λ antibody within live sample acquisition are indicated within the plot. **B**, Bar graph shows the area under the curve (AUC) of 4-OHT induced Ca^{2+} kinetics, representing autonomous BCR signalling ($p^*<0.05$; $p^{**}=0.0018$). **C**, Same as B, showing AUC of 4-OHT+anti-Igκ/λ antibody induced Ca kinetics representing BCR signaling strength ($p=0.1268$). In panels A, B and C, results are representative of mean ±SD of three independent experiments, showing each measurement, and analysed by One-Way ANOVA with Welch's approximation followed by Dunnett's T3 multiple comparison.

Editor's Summary
It is generally acknowledged that pathological B-cell receptors drive chronic lymphocytic leukaemia (CLL) via continuous signalling emanating from BCR-BCR homotypic interactions, rather than external antigens. Here the authors show, by analysing the structure and function of three B-cell receptors from patients with stereotyped CLL subset 1 that homotypic interactions and consequential autonomous signalling is not universal and other mechanisms could play roles in leukemic proliferation of CLL cells.

Peer review information: *Nature Communications* thanks Long Ma, Ludvig Munthe and the other, anonymous, reviewer(s) for their contribution to the peer review of this work. A peer review file is available.

A

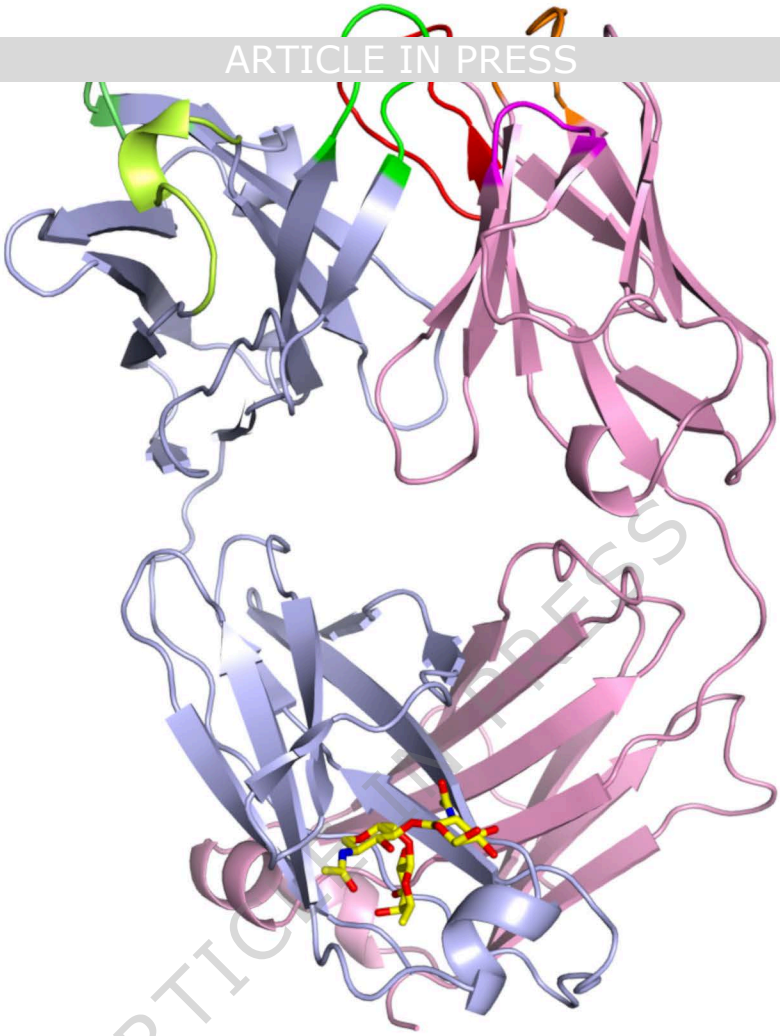

B

```
P3129       QVQLVQSGAEVKKPGASVKVSCKASGYTFTSYAMHWVRQAPGQRLEWMGWINAGNGNTKY   60
P10015      QVQLVQSGAEVKKPGASVKVSCKASGYTFTGYYMHWVRQAPGQGLEWMGWINPNSGGTNY   60
P1173       EVQLVQSGAEVKKPGESLRISCKGSGYSFTSYWITWVRQMPGKGLEWMGRIDPSDSYTNY   60
            :************** *:::***.***:**.* : **** **: ***** *: ... *:*

P3129       SQKFQGRVTITRDTSASTAYMELSSLRSEDTAVYYCAREQWLDLAHFDYWGQGTLVTVSS   120
P10015      AQKFQGRVTMTRDTSISTAYMELSRLRSDDTAVYYCARAQWLVVTNFDYWGQGTLVTVSS   120
P1173       SPSFQGHVTISADKSISTAYLQWSSLKASDTAMYYCAREQWLGIKNFDYWGQGTLVTVSS   120
            : .***:**:: *.* ****:: * *:::.***:***** *** : :**************

IGKV1-39    DIQMTQSPSSLSASVGDRVTITCRASQSISSYLNWYQQKPGKAPKLLIYAASSLQSGVPS   60
IGKV1-39    RFSGSGSGTDFTLTISSLQPEDFATYYCQQSYSTP                            105
```

A

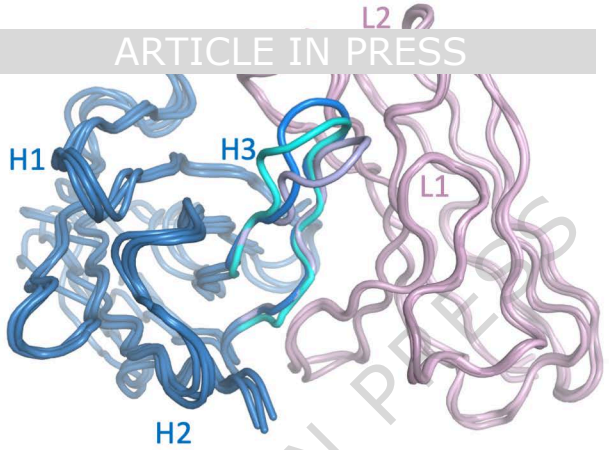

B

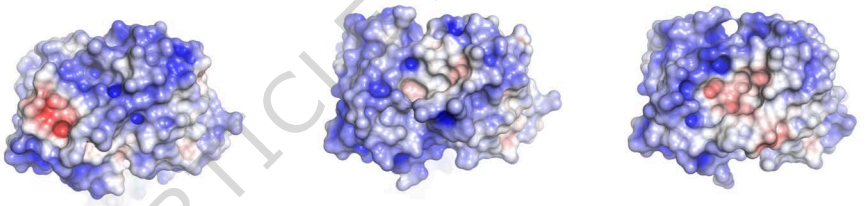

C

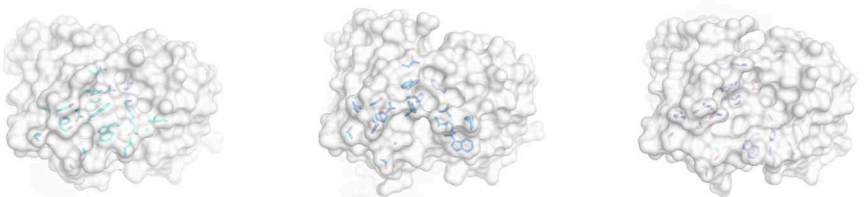

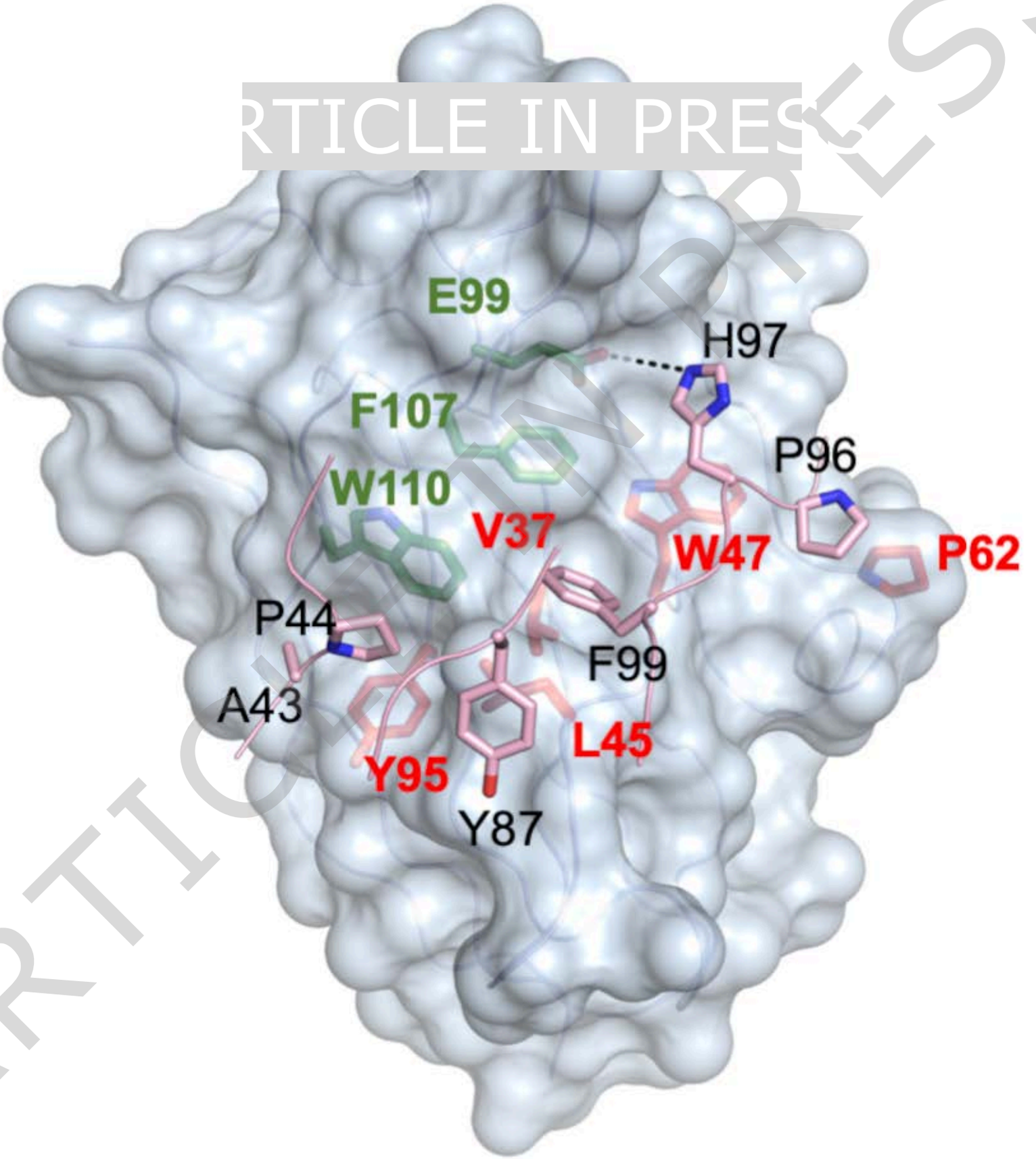

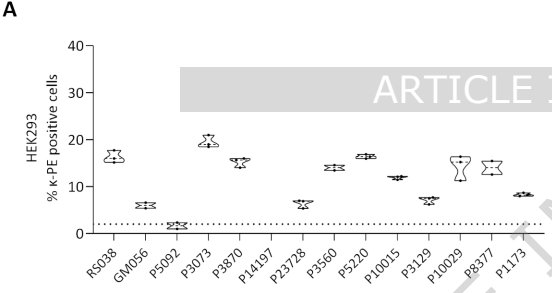

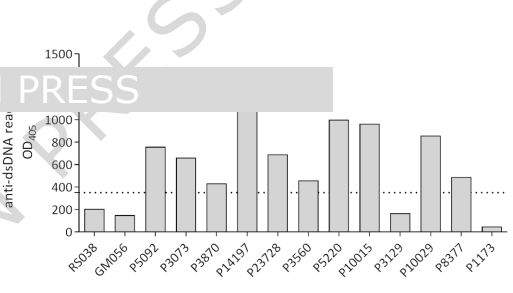

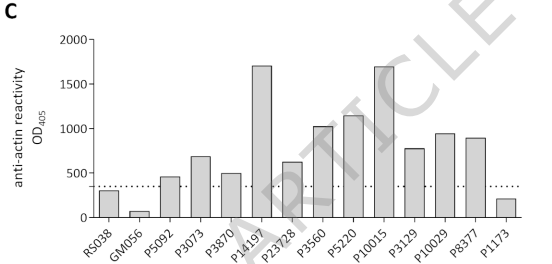

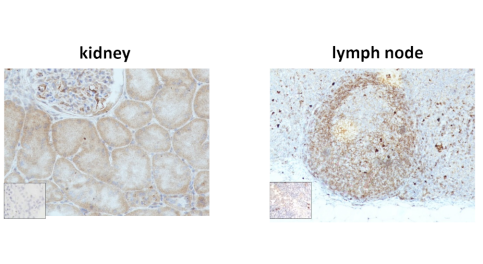

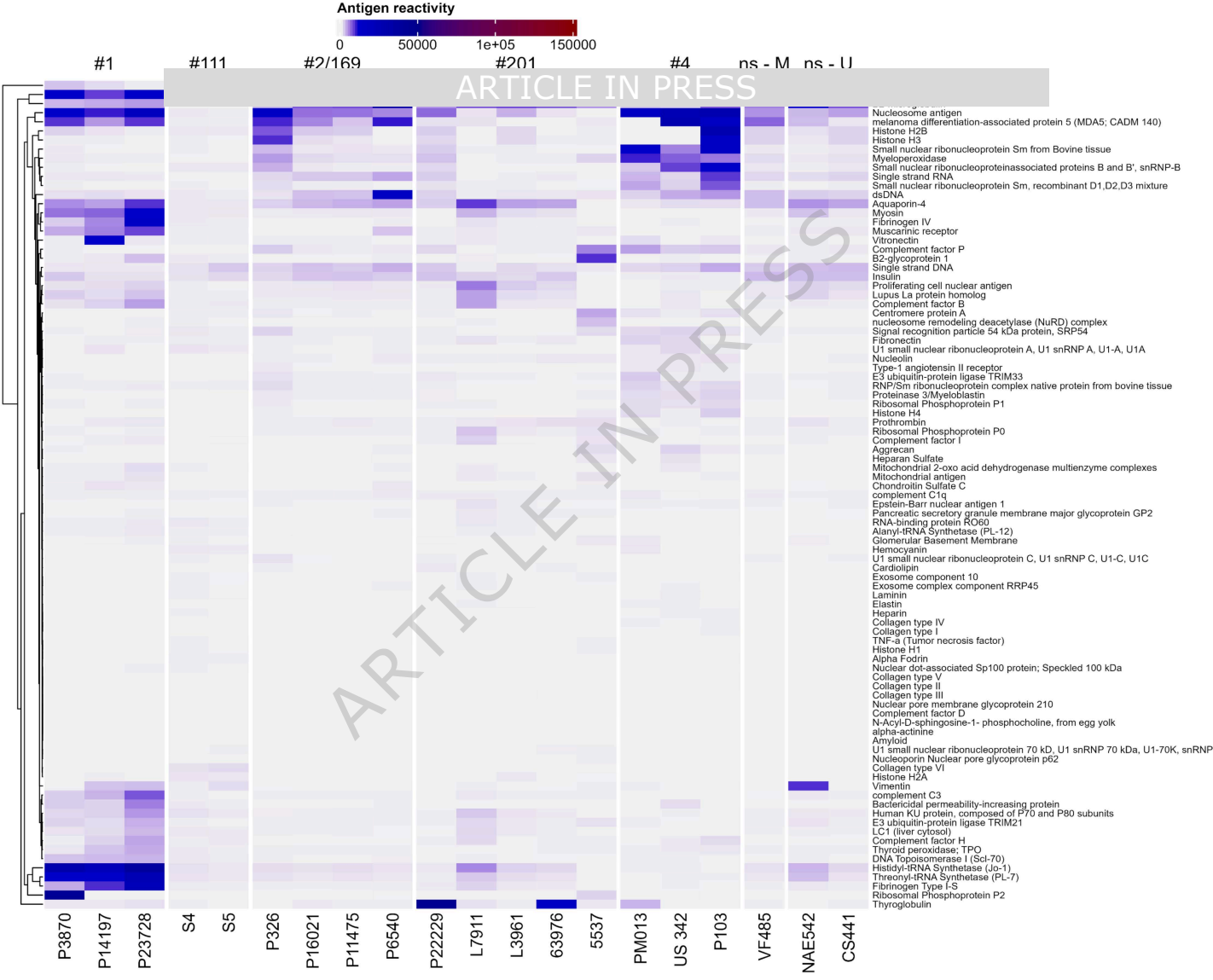

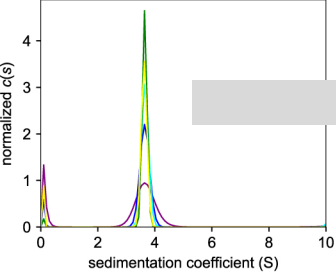

P3129

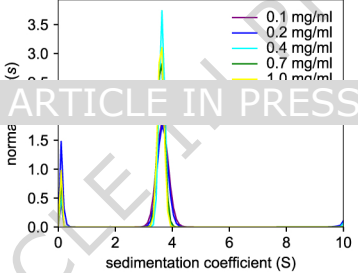

P10015

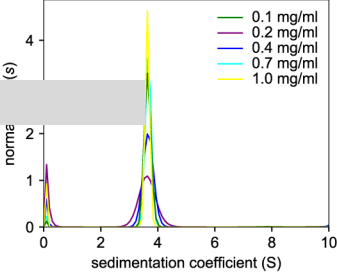

P1173